catalysts

MDPI

Article

Photocatalytic Activity of ZnO/Ag Nanoparticles Fabricated by a Spray Pyrolysis Method with Different O_2:N_2 Carrier Gas Ratios and Ag Contents

Meditha Hudandini [1], Nurdiana Ratna Puri [2], Sugeng Winardi [2], Widiyastuti Widiyastuti [2], Manabu Shimada [1] and Kusdianto Kusdianto [2,*]

[1] Chemical Engineering Program, Graduate School of Advanced Science and Engineering, Hiroshima University, 4-1, Kagamiyama 1-Chome, Higashi-Hiroshima 739-8527, Hiroshima, Japan
[2] Chemical Engineering Department, Institut Teknologi Sepuluh Nopember, Kampus ITS Sukolilo, Surabaya 60111, Indonesia
* Correspondence: kusdianto@chem-eng.its.ac.id

Abstract: Wastewaters of the textile industry, e.g., those generated in Gresik, Indonesia, are a possible threat to the environment and should be treated before disposal. Photodegradation is a more promising method to overcome this problem than conventional methods such as biodegradation. ZnO is widely used for photodegradation due to its unique physical and chemical properties and stability. In this study, Ag was loaded onto ZnO, which is non-toxic and inexpensive, can improve the electron–hole separation, and has a significant catalytic potential. Pristine ZnO and ZnO-Ag nanoparticles were fabricated by an ultrasonic spray pyrolysis system at different Ag contents (1, 5, and 10 wt%). The carrier gas ratio (O_2:N_2) was also changed (1:0, 1:2, 1:1, 2:1, and 0:1) to examine its effects on the nanoparticle characteristics. The nanoparticle characteristics were examined using X-ray diffraction (XRD), scanning electron microscopy (SEM), transmission electron microscopy (TEM), and Brunauer, Emmett, and Teller (BET) specific surface area. The results were interpreted in relation to photodegradation under UV light irradiation. An increase in the ZnO-Ag activity compared with pristine ZnO was observed at a carrier gas ratio of 0:1 with reaction rate constants of 0.0059 and 0.0025 min^{-1}, respectively.

Keywords: chemical vapor deposition (CVD); gas-phase; photodecomposition; specific surface area; nanocomposite

Citation: Hudandini, M.; Puri, N.R.; Winardi, S.; Widiyastuti, W.; Shimada, M.; Kusdianto, K. Photocatalytic Activity of ZnO/Ag Nanoparticles Fabricated by a Spray Pyrolysis Method with Different O_2:N_2 Carrier Gas Ratios and Ag Contents. *Catalysts* **2022**, *12*, 1374. https://doi.org/10.3390/catal12111374

Academic Editors: Jorge Bedia and Carolina Belver

Received: 3 October 2022
Accepted: 3 November 2022
Published: 5 November 2022

1. Introduction

The growth in the textile industry with its large water consumption impacts the environment because wastewater effluents contain large quantities of organic pollutions [1]. These compounds have highly toxic effects on living organisms [2]. Advanced oxidation processes (AOP) by photocatalysts have been considered for the treatment of dye-polluted wastewaters [1,3,4]. The advantages of AOP include (i) fast degradation of pollutants, (ii) complete mineralization of harmful organic wastes, (iii) operation at ambient temperature and pressure, and (iv) reduction of the toxicity of organic compounds [5]. The process of AOP mainly involves the generation of reactive hydroxyl radicals and its further functionalization to degrade organic compounds. Currently, most research focuses on photocatalytic oxidation using materials such as semiconductors [1,6].

ZnO (band gap energy = 3.37 eV) can degrade harmful organic compounds [3]. It is a semiconductor that is low-cost, is environmentally safe, and has good physical and chemical stability [2,7]. In addition, it has a high surface area and high photosensitivity [8]. However, the fast recombination of the excited electrons (e−) and holes (h+) due to its large band gap energy significantly limits the utilization of ZnO [7,8]. Nevertheless, several studies reported several methods, such as doping with metals, e.g., Au [8,9], Ag [8,10,11],

and Pt [10], to increase the functionality of ZnO. These metals can suppress the recombination of electrons and holes by acting as an electron sink for the excited electrons from the valence band of ZnO [8]. In this study, ZnO was loaded with Ag because of its photocatalytic potential, low-cost, and non-toxicity [2]. ZnO-Ag for photodegradation of organic pollutants has also been extensively studied because of its good performance [11].

Nanocomposite fabrication can be obtained by several methods in the liquid or gas phase. However, the liquid-phase method involves more steps than the gas-phase method. Gas-phase methods include spray pyrolysis, sputtering, and electron-beam evaporation [7]. In this study, ultrasonic spray pyrolysis is used for nanocomposite synthesis. This is a single-step fabrication process that results in a better dispersion of the produced nanomaterials, which further enhances its activity [12]. This method consists of generation of the droplets by a nebulizer followed by solvent evaporation, precursor chemical reaction, and densification of the formed particles [9,13].

Here, ultrasonic spray pyrolysis is used to fabricate pristine ZnO and ZnO-Ag nanoparticles. The process was optimized to produce desirable nanoparticles for the degradation of organic compounds. The nanoparticle formation or characteristics of the fabricated ZnO nanoparticles is affected by several parameters such as the precursor concentration [14], carrier gas flow rate [14,15], type of carrier gas used [16], and furnace temperature [14,17]. Several studies have used spray pyrolysis with different carrier gases. Different carrier gases generate different structures and properties of the nanocomposites. Air and nitrogen as carrier gases generated ZnO nanoparticles with different morphologies and resistivities [16]. Other studies that used materials such as ZnO/Mn, fabricated using oxygen, nitrogen, or air as the carrier gas, showed that the carrier gas type affected the magnetic characteristics of the nanocomposites, which is significantly affected by lower system temperatures [18]. Furthermore, other semiconductors, such as α-Ga_2O_3, was fabricated using different carrier gases. A carrier gas containing a high oxygen concentration generated higher crystallinity and better film quality [19]. Previous studies have shown the effect of different carrier gases used toward the characteristics of the produced nanoparticles. These effects may be further attributed to the reaction conditions based on the type of gas used. Air and oxygen create an oxidizing atmosphere for the reactions, whereas gases such as Ar or N_2 provide an inert reaction atmosphere. Thus, these two types of carrier gases produce different characteristics of the nanoparticles [13].

To the best of our knowledge, the effect of the carrier gas on the characteristics and photocatalytic activity of ZnO-Ag nanocomposites has not been explored in detail. This work provides a close examination of the characteristics of the produced nanoparticles fabricated using an ultrasonic spray pyrolysis method at different carrier gas ratios (oxygen to nitrogen). The morphology was observed using scanning electron microscopy (SEM) and transmission electron microscopy (TEM), and the elemental analysis was observed using energy dispersive spectroscopy (EDS). Furthermore, the crystallinity and crystallite size were investigated by X-ray diffraction (XRD), and the specific surface area (SBET) was studied by the nitrogen adsorption isotherm using the Brunauer Emmett and Teller (BET) method. The correlation of these characteristics with the carrier gas ratio (O_2:N_2) and the Ag contents (0, 1, 5, and 10 wt%) was investigated. Furthermore, the photocatalytic degradation of organic compounds in actual textile wastewaters using the produced nanoparticles was examined under UV light irradiation.

2. Results and Discussion

2.1. Morphological Analysis of the Produced Nanoparticles

Figure 1a–h shows the morphology of ZnO and ZnO-Ag nanoparticles synthesized by ultrasonic spray pyrolysis. The figure shows crumpled spherical secondary submicron particles. No significant morphological change is observed at different carrier gas ratios and Ag contents. The cumulative size distribution (Figure 1i,j) of the secondary submicron nanoparticles was also measured. The increase in the Ag content does not affect the size distribution; however, the diameters of the secondary particles slightly increased with the

increase in the nitrogen carrier gas ratio. The formation of these nanoparticles occurred during the evaporation of the solvent droplets in the aerosolized precursor followed by compression and decomposition of the precursor in the tubular furnace [20]. These morphological results agree well with previous studies. The formation of the nanoparticles and the obtained morphology are affected by several parameters such as the evaporation rate of the solvent and concentration of the precursor [12,21]. Upon evaporation, the confinement force, which compresses the droplets within the pathway, affects the morphology and size of the nanoparticles. The confinement force is proportional to the evaporation rate, which is significantly affected by the furnace temperature. A furnace temperature of 400 °C is sufficiently high to cause a significant water (solvent)-evaporation rate and the crumpled spherical structure of the nanoparticles. Furthermore, the precursor concentration is proportional to the confinement force and particle size. However, the confinement force is inversely proportional to the particle size. Thus, appropriate concentrations should be used to produce the desired morphology and size of nanoparticles.

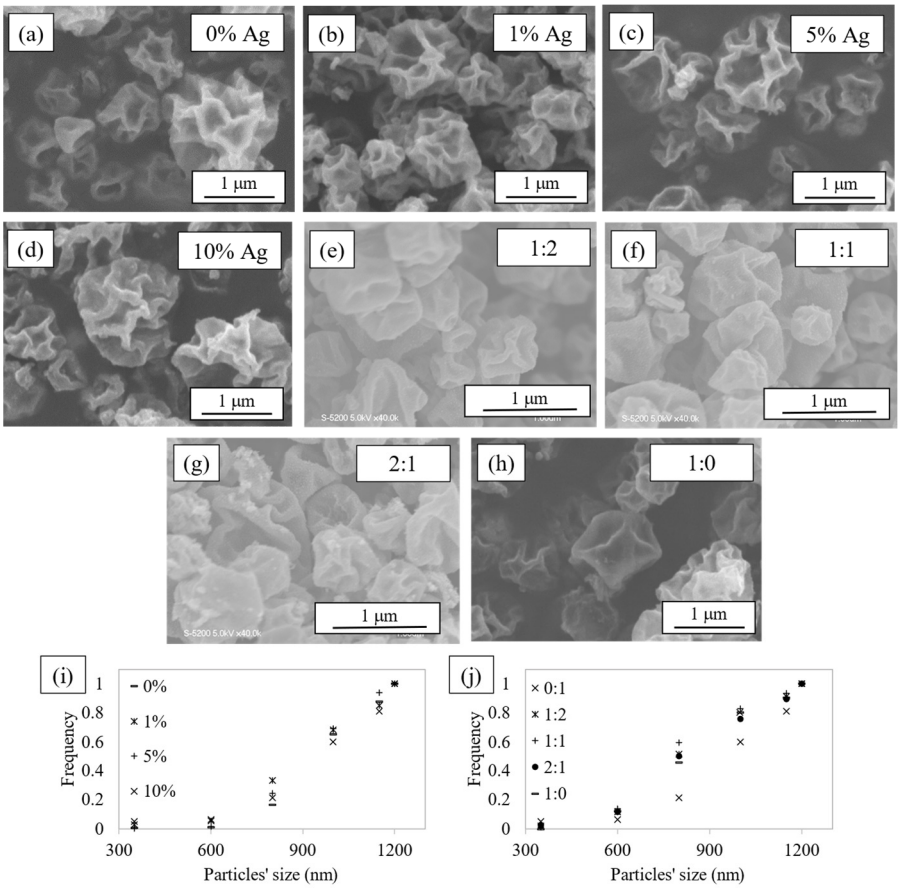

Figure 1. Morphology of (**a**) pristine ZnO, (**b**–**d**) ZnO-Ag with Ag content of (**b**) 1 wt%, (**c**) 5 wt%, (**d**) 10 wt% fabricated at an O_2:N_2 ratio of 0:1, (**e**–**h**) ZnO-Ag with Ag content of 10 wt% fabricated at different O_2:N_2 ratios, and (**i**,**j**) a cumulative size distribution of the nanoparticles.

TEM images (Figure 2a,b) show that the crumple-shaped spheres consisted of smaller primary nanoparticles. The EDS results (Figure 2c,d) indicated the presence of Zn, O, and Ag. In pristine ZnO, the ZnLα, ZnKα, ZnKβ, and OKα peaks confirm the presence of ZnO. The AgLα peak confirms the presence of Ag nanoparticles. The CuKα and CuKβ peaks correspond to the TEM grid that was used for observations in TEM measurements, and no impurities are observed in the samples.

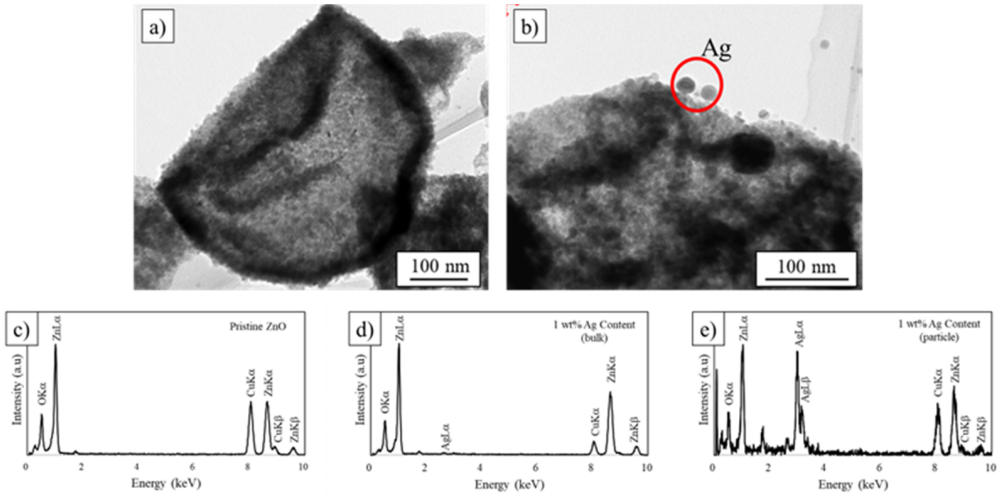

Figure 2. TEM-EDS of (**a**,**c**) Pristine ZnO and (**b**,**d**,**e**) ZnO-Ag nanoparticles at Ag content of 1 wt%.

2.2. Analysis of the Crystal Structure of the Produced Nanoparticles

The crystallization of the nanoparticles was observed using selected area electron diffraction (SAED) of ZnO-Ag (Figure 3a). The figure shows rings corresponding to the (100), (101), (102), and (110) lattice planes of wurtzite ZnO. The high-resolution TEM (HRTEM) image (Figure 3b) confirms the presence of the Ag nanoparticles and with a (111) crystal plane.

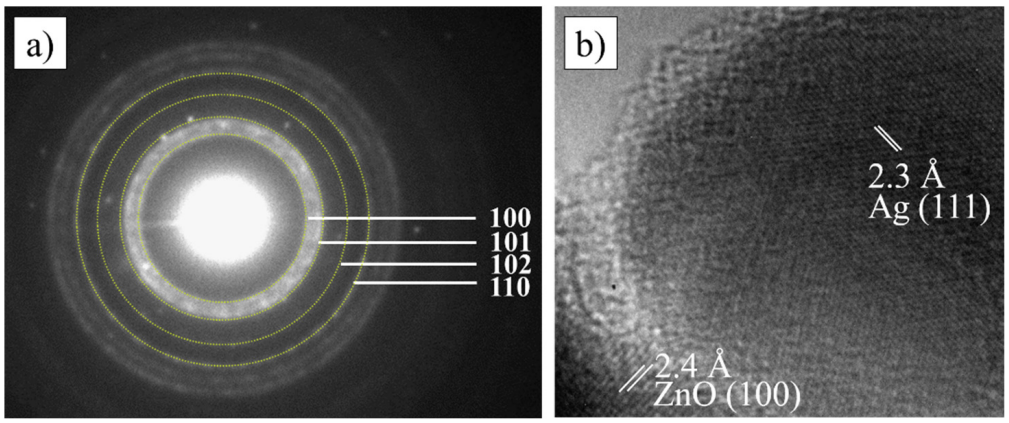

Figure 3. (**a**) SAED and (**b**) HR-TEM of ZnO-Ag nanoparticles at a Ag content of 1 wt%.

Hexagonal ZnO was identified by the XRD peaks (Figure 4) at 2θ = 31.5°, 33.9°, 35.8°, and 56.5° that correspond to the (100), (002), (101), and (110) crystal planes, respectively [6]. Zn peaks are observed with high nitrogen ratios (Figure 4a). During fabrication, zinc acetate dihydrate was used as the precursor, which decomposes to form Zn vapor at 400 °C, and when enough oxygen is present, ZnO is formed [22]. The Ag peak could only be observed at high Ag contents, either for oxygen or nitrogen-rich ratios, with the FCC peak of Ag observed at 2θ = 37.82° for the (111) crystal plane [6,23]. These XRD peaks prove the existence and successful formation of crystallized ZnO and Ag nanoparticles from the decomposition of zinc acetate dihydrate and silver nitrate by spray pyrolysis for both nitrogen- and oxygen-rich ratios.

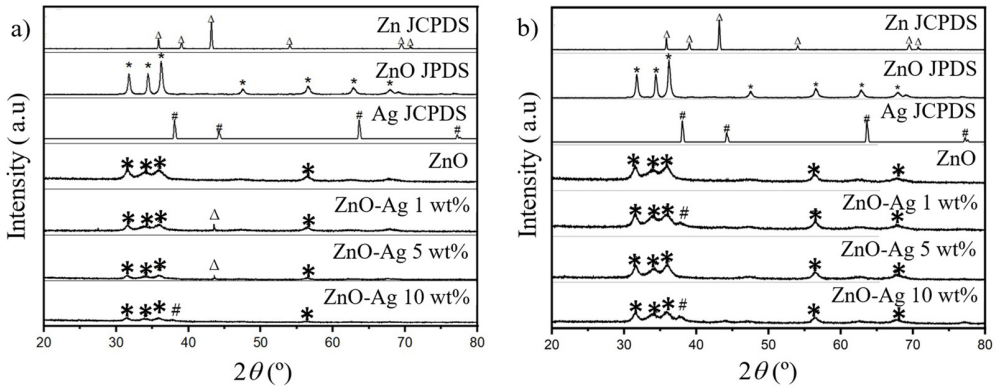

Figure 4. Crystalline phase of ZnO and ZnO-Ag fabricated at a carrier gas (O_2:N_2) ratio of (**a**) 0:1 and (**b**) 1:0. (symbols correspond to Δ Zn, * ZnO, and # Ag).

The crystallite size of ZnO was calculated using Scherrer's Equation (1). Figure 5 indicates that the crystallite size in a nitrogen-rich system that has not significantly changed with the addition of Ag to the ZnO nanoparticles. The crystallite size continues to increase with the increase in the oxygen ratio of the carrier gas. However, at a higher oxygen ratio, the crystallite size of pristine ZnO and the nanocomposite decreases. This is in accordance with the report by Li, et al. [24], such that for annealed ZnO under air, N_2, O_2 and vacuum following the grain size for air > N_2 > O_2 > vacuum, the existence of oxygen in the system was reported to suppress the grain growth by pinning the grain boundaries. At higher oxygen ratios, however, pristine ZnO nanoparticles have a slightly lower crystallite size than the ZnO-Ag nanocomposites. In this study, the presence of Ag nanoparticles affects the increase in the crystallite size of ZnO nanoparticles, especially at high oxygen ratios in the carrier gas. The increase in ZnO size with the addition of Ag in the oxygen-rich system can be explained by the more prominent effects of Ag doping toward ZnO in the oxygen, which may influence the crystal of ZnO nanoparticles [25]. Instead of following the significant decrease in size of pristine ZnO in higher oxygen ratios, the addition of Ag gave a higher crystallite size compared to pristine ZnO.

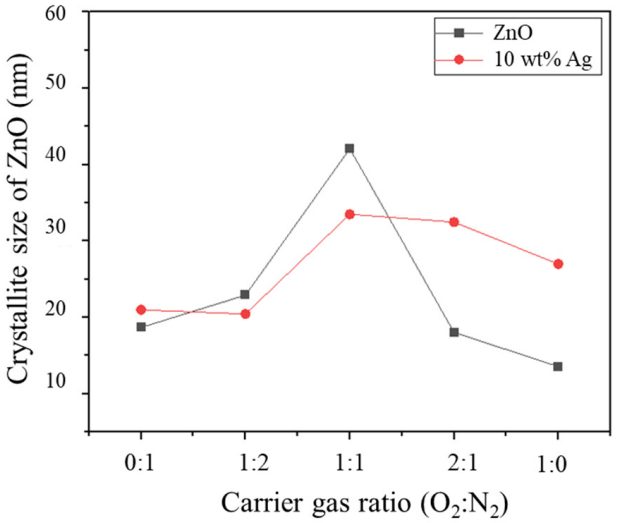

Figure 5. Crystallite size of ZnO at different carrier gas ratios and Ag contents.

2.3. Surface Area of the Produced Nanoparticles

The SBET of the nanoparticles was obtained using a nitrogen adsorption BET method. The surface area of the nanoparticles can significantly affect their photocatalytic activity. Tightly packed structure of the nanoparticles has a high surface area and free volume, which significantly increase their photocatalytic activity [21]. High surface area increases

the contact between the active sites of the nanoparticles with pollutants, which can optimize the degradation of the organic compounds [12]. Figure 6 indicates that, except for samples with 5 wt% Ag content, SBET decreases with the increase in the oxygen ratio. The largest SBET is measured at a Ag content of 10 wt% using only nitrogen as the carrier gas. In general, a pure nitrogen carrier gas exhibits a larger SBET than that of samples produced with the mixture or pure oxygen carrier gas. However, this is not consistent with the size change of the secondary nanoparticles, of which the size increase should have decreased SBET. This difference in the results can be attributed to the crumpled sphere shape of the nanoparticles developed in this study.

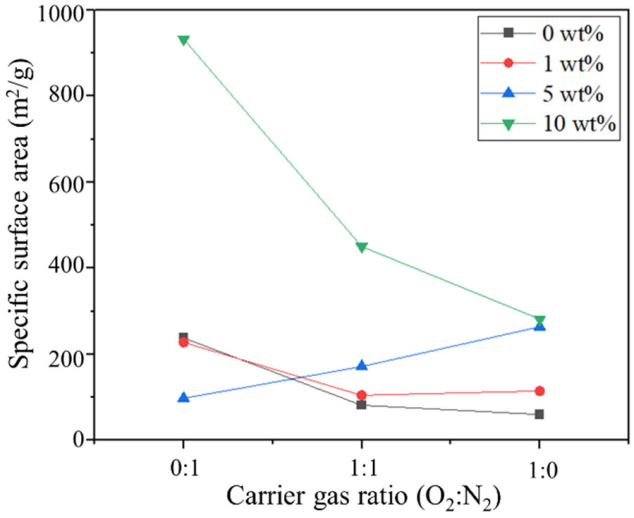

Figure 6. Specific surface area of ZnO and ZnO-Ag at different Ag contents and carrier gas (O_2:N_2) ratios.

Furthermore, the difference in SBET can be explained by the mechanism of the nanoparticle growth in the tubular furnace, in which the carrier gas atmosphere is expected to change the average temperature in the chamber and the evaporation rate of the solution [16]. Nitrogen has lower thermal conductivity than oxygen, which results in a lower evaporation rate, leading to the formation of non-aggregated nanoparticles. Aggregated nanoparticles tend to have lower surface area than non-aggregated nanoparticles.

2.4. Photocatalytic Activity of Pristine ZnO and ZnO-Ag at Different Carrier Gas Ratios

The photocatalytic activity of pristine ZnO and ZnO-Ag nanoparticles was studied for the degradation of textile wastewater under UV light irradiation. The process involves the decomposition of organic pollutants in the wastewater to less harmful compounds or minerals [26]. Figure 7 illustrates the effect of Ag content and type of carrier gas on the degradation reaction rate constant. Different Ag contents (0–10 wt%) and carrier gas ratios exhibited similar tendencies of rate constants, where the pure nitrogen carrier gas has the highest photocatalytic activity in all samples. As previously discussed, the carrier gas used in the system may affect several characteristics of the produced nanoparticles. The increase in the nitrogen ratio in the system increases the nanoparticle SBET. High SBET values can enhance the photocatalytic activity. Zn metal is also observed in the nanoparticles of the systems with higher nitrogen ratios. The synergetic effect of Zn can suppress the electron–hole recombination and further enhance the photocatalytic activity compared to pristine ZnO nanoparticles [27]. At 10 wt%, the effect of the carrier gases on the photocatalytic activity is more pronounced than at lower Ag contents. However, the reason for this phenomenon is still not clear. Thus, the Ag content and carrier gas type have a significant effect on the photocatalytic activity of the developed nanoparticles.

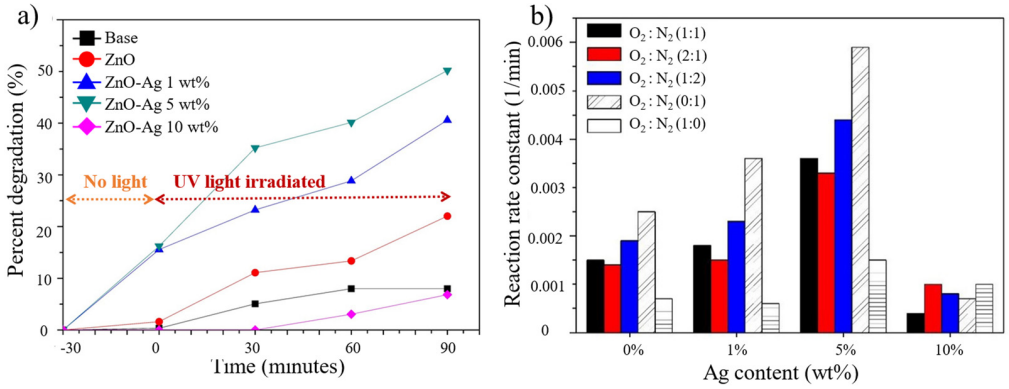

Figure 7. (**a**) Photocatalytic degradation percentage of the pollutants using ZnO-Ag synthesized by pure nitrogen as the carrier gas and (**b**) reaction rate constant of the produced nanoparticles under UV light irradiation.

The absorbance of the prepared samples with the mixed carrier gases and Ag contents were observed (Figure 8). The absorbance can be used to estimate the band gap energy (Figure 9) from $(\alpha hv)^n = A(hv - E_g)$, where α, hv, A, and Eg are the absorption, photon energy, constant, and band gap, respectively [28]. The absorbance measurement showed good response to the shorter wavelength of light, which indicated better performance under UV light irradiation. In addition, the existence of Ag metal nanoparticles was also proven from the absorbance spectra, with Ag metal nanoparticle peaks at wavelengths of 350–400 nm, which is a result from the localized plasmon resonance of Ag metal nanoparticles. The band gap energy of pristine ZnO showed a lower band gap energy of 3 eV compared to the typical band gap energy of ZnO that is 3.37 eV. A slight decrease in band gap energy with the increase in Ag content can be observed, which indicates a good photo response with increase in Ag content.

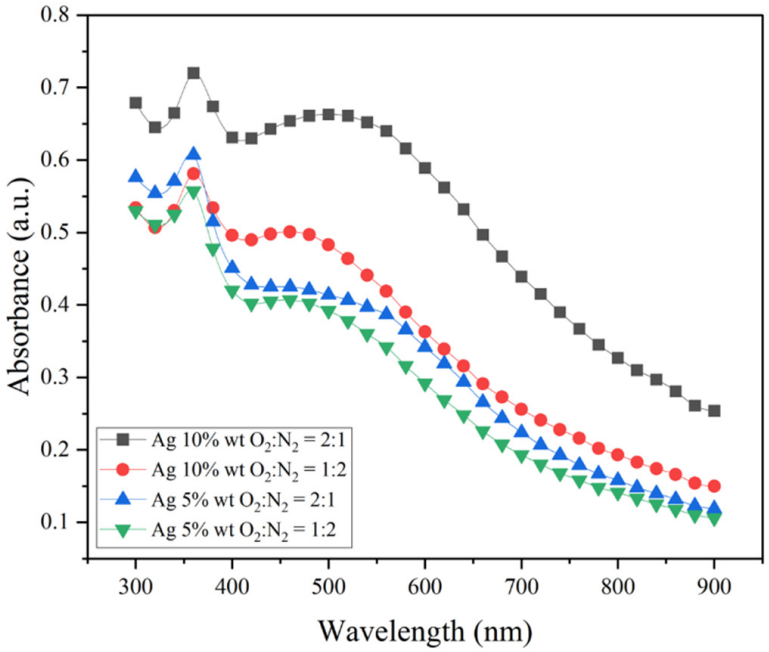

Figure 8. Absorbance spectra of ZnO-Ag nanoparticles with different carrier gas ratios and Ag contents.

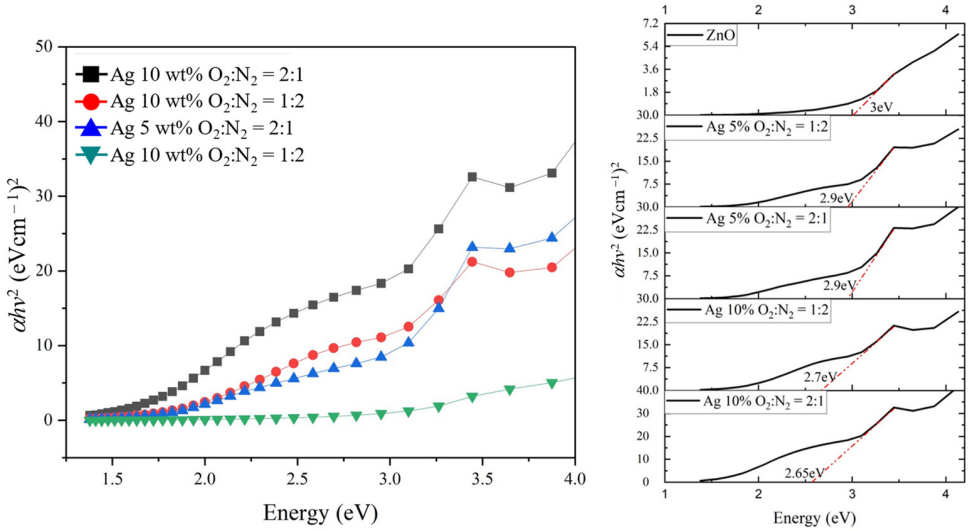

Figure 9. Band gap of ZnO-Ag nanoparticles with different carrier gas ratios and Ag contents.

Despite the higher surface area and lower band gap energy obtained with a Ag content of 10 wt%, the optimum photocatalytic activity is obtained at a Ag content of 5 wt%. This could be attributed to the excessive amount of Ag at a Ag content of 10 wt%, which also acts as charge recombination centers. The negatively charged Ag increases the capturing of holes, which reduces the electron–hole separation and hence decreases the degradation of organic compounds [12,29]. In addition, the increase in foreign material can decrease the photocatalytic activity because of the shielding effect toward the active sites of the photocatalyst [28]. Thus, this photocatalytic degradation is affected by several parameters such as the surface area [2,12], crystallinity [26], crystallite size [6] of ZnO as well as the concentration of the loaded materials [2]. The possible photocatalytic activity of ZnO is described by other research as shown below [8].

$ZnO + hv\ (UV) \rightarrow ZnO\ (e_{CB}^{-} + h_{VB}^{+})$

$h_{VB}^{+} + OH^{-} \rightarrow {}^{\bullet}OH$

$e_{CB}^{-} + O_2 \rightarrow {}^{\bullet}O_2$

${}^{\bullet}O^{-} + 2H^{+} \rightarrow 2{}^{\bullet}OH$

${}^{\bullet}OH + \text{organic pollutants} \rightarrow 2{}^{\bullet}OH$

The UV photon energy excites the electrons from the valence band of ZnO, which induces the formation of holes. These holes react with the existing OH^{-}, forming ${}^{\bullet}OH$ radicals. Furthermore, electrons can react with oxygen to form ${}^{\bullet}OH$ radicals. These species are known to have significant roles in the degradation process.

3. Materials and Methods

3.1. Preparation Methods

Nanoparticles were formed using an ultrasonic spray pyrolysis system (Figure 10) following the experimental method given in our previous study [4]. Zinc acetate dehydrate crystals ($Zn(CH_3COO)_2{\cdot}2H_2O$, 99.5%, E. Merck, D-6100 Darmstadt, FR Germany) were used as the precursor to fabricate ZnO nanoparticles. Distilled water was added to the powder to form a zinc acetate aqueous solution (0.1 M). To uniformly dissolve zinc acetate, the solution was ultrasonicated for 30 min. Afterward, the aqueous solution was continuously fed to the nebulizer using a peristaltic pump (Omron, NE-U17, Kyoto, Japan). The precursor was aerosolized, and the produced droplets were continuously carried to the tubular furnace by the carrier gas at a total flow rate of 2 L/min. Various ratios of O_2:N_2 were used in the carrier gas (1:0, 1:2, 1:1, 2:1, and 0:1). The tubular furnace temperature was maintained at 400 °C. Evaporation of the solvent and decomposition of the precursor to form nanoparticles occurred inside the furnace. The produced nanoparticle powder was

collected in the electrostatic precipitator at an applied voltage of 40 kV and a temperature of 120 °C, which was maintained to ensure that there was no condensation.

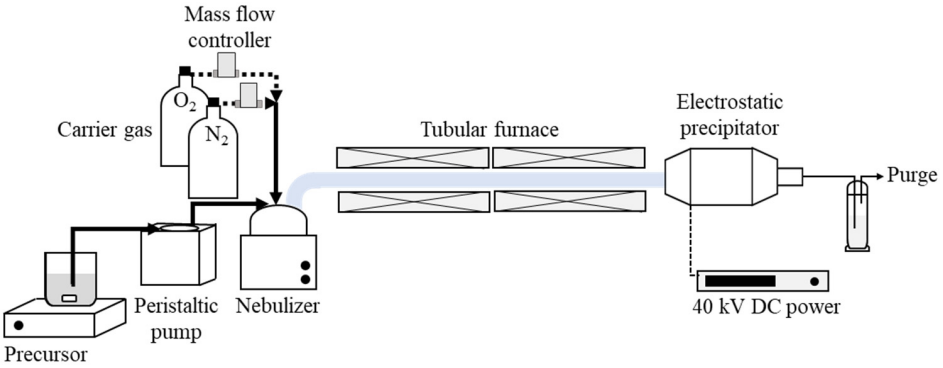

Figure 10. Experimental setup of the nanoparticle synthesis using a spray pyrolysis method.

ZnO-Ag nanocomposites were fabricated by adding silver nitrate ($AgNO_3$, 99.5%, E. Merck, D-6100 Darmstadt, FR Germany) at concentrations of 1, 5, and 10 wt% to the zinc acetate solution. The same method mentioned above was used to fabricate and collect the ZnO-Ag nanocomposite.

3.2. Materials Characterization

The particle morphology was observed using SEM (FlexSEM1000, Hitachi High Technologies, Tokyo, Japan), and further observation of the morphology and elemental analysis was conducted by TEM-EDS (JEM-2010, JEOL, Tokyo, Japan). The crystallinity and phase composition of the nanoparticles were determined by XRD (Philip XPERT MPD, Philips, Almelo, The Netherlands) operated at a 40 kV and 30 mA. The XRD patterns were obtained within a 2θ range of 20–80°. The crystallite size (D) of the nanoparticles was determined by the Scherrer formula shown below:

$$D = \frac{k\,\lambda}{B\,cos\,\theta} \quad (1)$$

where k is a constant (k = 0.9), λ is the X-ray wavelength (λ = 0.154 nm), B is the full width at half maximum of the peak, and θ is the XRD peak angle [6,23]. Furthermore, The SBET of the nanoparticles was determined by a nitrogen gas adsorption device (Quantachrome Instruments, Boynton Beach, FL, USA) based on the BET method.

3.3. Photocatalytic Test

The photocatalytic activity of the nanoparticles was tested for the degradation of organic dye pollutants found in real textile wastewater obtained from UD, ATBM Jufri Hartono, Gresik, East Java. The wastewater was firstly 10× diluted by the as-received distilled water. Next, the diluted pollutant solution (30 mL) was poured inside a beaker glass, in which the nanoparticle powder (10 mg) was added and continuously stirred throughout the photocatalytic test. The sample was placed in a dark chamber for 30 min to obtain the adsorption–desorption equilibrium of the photocatalyst and dye pollutants. The photocatalytic test was conducted for 90 min, in which the absorbance was measured at 30 min intervals using a UV–Vis spectrophotometer. The sample was centrifuged at 5000 rpm for each measurement to separate the powder catalyst from the liquid pollutant. The absorbance of the obtained supernatant was then measured using the UV–Vis spectrophotometer. The concentration of the dye is proportional to the measured intensity [26]. Thus, the reaction rate constant was calculated based on the slope of the dye concentration–intensity curve, i.e., $\ln(C_t/C_o) = kt$ [30], where k, t, C_t, and C_o are the reaction rate constant, reaction time, final concentration, and initial concentration, respectively.

4. Conclusions

Crumpled pristine ZnO and ZnO-Ag nanoparticles with high surface area were fabricated by a one-step ultrasonic spray pyrolysis method at different Ag contents and O_2:N_2 carrier gas ratios. The carrier gas ratio did not significantly affect the morphology, crystallite phase, or primary size of the nanoparticles. However, the SBET and photocatalytic activity of the nanoparticles changed with the increase in the nitrogen ratio. The nanoparticles exhibited good performance, and optimum activity (reaction rate constant = 0.0059 min^{-1}) was observed for the ZnO nanoparticles with a Ag content of 5 wt%, which were fabricated in a nitrogen-rich system.

Author Contributions: Conceptualization, K.K. and S.W.; Methodology, K.K., W.W. and M.H.; Formal analysis, M.H., N.R.P., W.W., M.S. and K.K.; Investigation, K.K., N.R.P. and M.H.; Writing—M.H.; Writing—review and editing, K.K., M.H. and M.S.; Supervision: K.K. and S.W. All authors have read and agreed to the published version of the manuscript.

Funding: Financial support from DRPM Kementrian Pendidikan, Kebudayaan, Riset dan Teknologi Indonesia with contract numbers: 084/E5/PG.02.00.PT/2022 and 1491/PKS/ITS/2022 through "Penelitian Dasar Unggulan Perguruan Tinggi" scheme. This research was also partly supported by Japan Society for the Promotion of Science (KAKENHI grant; grant number JP21K04750).

Data Availability Statement: In this manuscript, our characterizations were SEM, XRD, TEM, BET, and UV Vis. All data have been reported as the images.

Acknowledgments: Our biggest gratitude goes to the persons who supported this research, to Timotius Candra Kusuma, Nungki Widya Savitri, and Syamsul Muarafi Subekhi for the experimental assistance, and to UD. ATBM Jufri Hartano for providing the tested wastewater.

Conflicts of Interest: The authors declare no conflict of interest.

References

1. Paździor, K.; Bilińska, L.; Ledakowicz, S. A review of the existing and emerging technologies in the combination of AOPs and biological processes in industrial textile wastewater treatment. *Chem. Eng. J.* **2019**, *376*, 120597. [CrossRef]
2. Saravanan, R.; Karthikeyan, N.; Gupta, V.; Thirumal, E.; Thangadurai, P.; Narayanan, V.; Stephen, A. ZnO/Ag nanocomposite: An efficient catalyst for degradation studies of textile effluents under visible light. *Mater. Sci. Eng. C* **2013**, *33*, 2235–2244. [CrossRef] [PubMed]
3. Akkari, M.; Aranda, P.; Belver, C.; Bedia, J.; Amara, A.B.H.; Ruiz-Hitzky, E. ZnO/sepiolite heterostructured materials for solar photocatalytic degradation of pharmaceuticals in wastewater. *Appl. Clay Sci.* **2018**, *156*, 104–109. [CrossRef]
4. Kusdianto, K.; Hudandini, M.; Kusuma, T.C.; Widiyastuti, W.; Madhania, S.; Machmudah, S.; Nurtono, T.; Puspitasari, D.; Winardi, S. Photocatalytic degradation of organic waste derived from textile dye by ZnO-Ag nanocomposite synthesized by spray pyrolysis. *AIP Conf. Proc.* **2020**, *2219*, 30001.
5. Ong, C.B.; Ng, L.Y.; Mohammad, A.W. A review of ZnO nanoparticles as solar photocatalysts: Synthesis, mechanisms and applications. *Renew. Sustain. Energy Rev.* **2018**, *81*, 536–551. [CrossRef]
6. El-Bindary, A.A.; El-Marsafy, S.M.; El-Maddah, A.A. Enhancement of the photocatalytic activity of ZnO nanoparticles by silver doping for the degradation of AY99 contaminants. *J. Mol. Struct.* **2019**, *1191*, 76–84. [CrossRef]
7. Kusdianto, K.; Sari, T.D.; Laksono, M.A.; Madhania, S.; Winardi, S. Fabrication and application of ZnO-Ag nanocomposite materials prepared by gas-phase methods. *IOP Conf. Ser. Mater. Sci. Eng.* **2021**, *1053*, 12023. [CrossRef]
8. Fageria, P.; Gangopadhyay, S.; Pande, S. Synthesis of ZnO/Au and ZnO/Ag nanoparticles and their photocatalytic application using UV and visible light. *RSC Adv.* **2014**, *4*, 24962–24972. [CrossRef]
9. Lee, Y.; Fujimoto, T.; Yamanaka, S.; Kuga, Y. Evaluation of photocatalysis of Au supported ZnO prepared by the spray pyrolysis method. *Adv. Powder Technol.* **2021**, *32*, 1619–1626. [CrossRef]
10. Muñoz-Fernandez, L.; Sierra-Fernandez, A.; Milošević, O.; Rabanal, M.E. Solvothermal synthesis of Ag/ZnO and Pt/ZnO nanocomposites and comparison of their photocatalytic behaviors on dyes degradation. *Adv. Powder Technol.* **2016**, *27*, 983–993. [CrossRef]
11. Zhang, Q.; Li, J.; Xu, M. Ag-decorated ZnO-based nanocomposites for visible light-driven photocatalytic degradation: Basic understanding and outlook. *J. Phys. D Appl. Phys.* **2022**, *55*, 483001. [CrossRef]
12. Dermenci, K.B.; Genc, B.; Ebin, B.; Olmez-Hanci, T.; Gürmen, S. Photocatalytic studies of Ag/ZnO nanocomposite particles produced via ultrasonic spray pyrolysis method. *J. Alloys Compd.* **2014**, *586*, 267–273. [CrossRef]
13. Leng, J.; Wang, Z.; Wang, J.; Wu, H.-H.; Yan, G.; Li, X.; Guo, H.; Liu, Y.; Zhang, Q.; Guo, Z. Advances in nanostructures fabricated via spray pyrolysis and their applications in energy storage and conversion. *Chem. Soc. Rev.* **2019**, *48*, 3015–3072. [CrossRef]

14. Emil, E.; Alkan, G.; Gurmen, S.; Rudolf, R.; Jenko, D.; Friedrich, B. Tuning the Morphology of ZnO Nanostructures with the Ultrasonic Spray Pyrolysis Process. *Metals* **2018**, *8*, 569. [CrossRef]
15. Iskandar, F. Nanoparticle processing for optical applications—A review. *Adv. Powder Technol.* **2009**, *20*, 283–292. [CrossRef]
16. Jongthammanurak, S.; Witana, M.; Cheawkul, T.; Thanachayanont, C. The effects of carrier gas and substrate temperature on ZnO films prepared by ultrasonic spray pyrolysis. *Mater. Sci. Semicond. Process.* **2013**, *16*, 625–632. [CrossRef]
17. Wittawat, R.; Rittipun, R.; Jarasfah, M.; Nattaporn, B. Synthesis of ZnO/TiO_2 spherical particles for blue light screening by ultrasonic spray pyrolysis. *Mater. Today Commun.* **2020**, *24*, 101126. [CrossRef]
18. Vorovsky, V.Y.; Kovalenko, A.V.; Kushneryov, A.I.; Khmelenko, O.V. Preparation of zinc oxide nanopowders doped with manganese, which have ferromagnetic properties at room temperature. *Funct. Mater.* **2018**, *25*, 61–66. [CrossRef]
19. Xu, Y.; Zhang, C.; Cheng, Y.; Li, Z.; Cheng, Y.; Feng, Q.; Chen, D.; Zhang, J.; Hao, Y. Influence of Carrier Gases on the Quality of Epitaxial Corundum-Structured α-Ga_2O_3 Films Grown by Mist Chemical Vapor Deposition Method. *Matererials* **2019**, *12*, 3670. [CrossRef]
20. Rahemi Ardekani, S.; Sabour Rouhaghdam, A.; Nazari, M. N-doped ZnO-CuO nanocomposite prepared by one-step ultrasonic spray pyrolysis and its photocatalytic activity. *Chem. Phys. Lett.* **2018**, *705*, 19–22. [CrossRef]
21. El Rouby, W.M.A. Crumpled graphene: Preparation and applications. *RSC Adv.* **2015**, *5*, 66767–66796. [CrossRef]
22. Wang, R.-C.; Tsai, C.-C. Efficient synthesis of ZnO nanoparticles, nanowalls, and nanowires by thermal decomposition of zinc acetate at a low temperature. *Appl. Phys. A* **2009**, *94*, 241–245. [CrossRef]
23. Kusdianto, K.; Hudandini, M.; Jiang, D.; Kubo, M.; Shimada, M. Effect of Heating Rate on the Photocatalytic Activity of Ag–TiO_2 Nanocomposites by One-Step Process via Aerosol Routes. *Catalysts* **2021**, *12*, 17. [CrossRef]
24. Li, J.; Huang, J.-H.; Zhang, Y.-L.; Yang, Y.; Song, W.-J.; Li, X.-M. Effects of rapid thermal annealing in different ambients on structural, electrical, and optical properties of ZnO thin films by sol-gel method. *J. Electroceramics* **2011**, *26*, 84–89. [CrossRef]
25. Yan, Y.; Al-Jassim, M.M.; Wei, S.H. Doping of ZnO by group-IB elements. *Appl. Phys. Lett.* **2006**, *89*, 181912. [CrossRef]
26. Tripathy, N.; Ahmad, R.; Kuk, H.; Lee, D.H.; Hahn, Y.-B.; Khang, G. Rapid methyl orange degradation using porous ZnO spheres photocatalyst. *J. Photochem. Photobiol. B Biol.* **2016**, *161*, 312–317. [CrossRef]
27. Ma, H.; Yue, L.; Yu, C.; Dong, X.; Zhang, X.; Xue, M.; Zhang, X.; Fu, Y. Synthesis, characterization and photocatalytic activity of Cu-doped Zn/ZnO photocatalyst with carbon modification. *J. Mater. Chem.* **2012**, *22*, 23780–23788. [CrossRef]
28. Liu, C.; Mao, S.; Wang, H.; Wu, Y.; Wang, F.; Xia, M.; Chen, Q. Peroxymonosulfate-assisted for facilitating photocatalytic degradation performance of 2D/2D WO_3/BiOBr S-scheme heterojunction. *Chem. Eng. J.* **2022**, *430*, 132806. [CrossRef]
29. Georgekutty, R.; Seery, M.K.; Pillai, S.C. A Highly Efficient Ag-ZnO Photocatalyst: Synthesis, Properties, and Mechanism. *J. Phys. Chem. C* **2008**, *112*, 13563–13570. [CrossRef]
30. Kusdianto, K.; Jiang, D.; Kubo, M.; Shimada, M. Effect of annealing temperature on the photocatalytic activity of Ag–TiO_2 nanocomposite films by one-step gas-phase deposition. *Mater. Res. Bull.* **2018**, *97*, 497–505. [CrossRef]